ELSEVIER

Materials Science and Engineering B 137 (2007) 189–194

MATERIALS SCIENCE & ENGINEERING B

www.elsevier.com/locate/mseb

Sol–gel auto-combustion synthesis of samarium-doped TiO_2 nanoparticles and their photocatalytic activity under visible light irradiation

Qi Xiao [a,b,*], Zhichun Si [a], Zhiming Yu [b], Guanzhou Qiu [a]

[a] *School of Resources Processing and Bioengineering, Central South University, Changsha 410083, China*
[b] *School of Materials Science and Engineering, Central South University, Changsha 410083, China*

Received 10 August 2006; received in revised form 4 November 2006; accepted 6 November 2006

Abstract

High photocatalytic activity of Sm^{3+}-doped TiO_2 nanocrystalline under visible light has been successfully prepared by sol–gel auto-combustion technique. The samples were characterized by X-ray diffraction, UV–vis diffuse reflectance spectroscopy and photoluminescence (PL) spectra. UV–vis diffuse reflectance spectra showed a slight shift to longer wavelengths and an extension of the absorption in the visible region for almost all the samarium-doped samples, compared to the non-doped sample. The results of photocatalytic decomposition of methylene blue (MB) over 0.5 mol% Sm^{3+}-TiO_2 prepared at various calcinations temperatures show that the sample calcinated at 600 °C consists of mixed phases with 51.61% rutile shows the highest photocatalytic activity, which suggests the existence of a synergistic effect between anatase and rutile powders under visible light. Doping with the samarium ions significantly enhanced the overall photocatalytic activity for MB degradation under visible light irradiation because the larger specific surface area and the higher separation efficiency of electron–hole pairs were obtained simultaneously for Sm^{3+}-doped TiO_2 nanocrystalline. It was found that there were certain relationships between PL spectra and photocatalytic activity, namely, the stronger the PL intensity, the larger the content of oxygen vacancies and defects, the higher the photocatalytic activity. Therefore, in this study, 0.5 mol% may be the most suitable content of Sm^{3+} in the titania, at which the recombination of photoinduced electrons and holes could be effectively inhibited and thereby the highest photocatalytic activity is formed.

Keywords: Samarium-doped TiO_2; Sol–gel auto-combustion synthesis; Visible light; Photocatalytic activity

1. Introduction

TiO_2-based photocatalytic oxidation techniques have received much attention due to their promising potential in application for complete mineralization of many toxic and non-biodegradable organics [1–3]. Due to the large band gap (∼3.2 eV) all photon-driven applications of TiO_2 require ultraviolet light for excitation. Despite the promising properties, application is now limited, for the UV region occupies only near 4% of the entire solar spectrum, while 45% of the energy belongs to visible light. More practical applications can be achieved if the photocatalytic active region can be expanded to the visible light region (400–700 nm); the photoenergy can be used more efficiently. Therefore, in order to realize the solar decontamination process, many efforts have been made to prepare TiO_2 photocatalysts that can drive the photodegradation reaction under visible light, including dye sensitization [4], external surface modifications [5,6], or band gap tailoring. For the first two cases, there are some problems including the instability of the organic complex and the complexity of materials synthesis. Band gap tailing by doping is the most efficient and frequently used method. Doping, within certain limits, serves to prolong the lifetime of charge carriers if the dopants have energy levels just below the conduction band or just above the valence band of to realize shallow charge carrier trapping. As reported in the literature, transition metals doping (e.g., Co, Fe) [7,8], non-metallic elements doping (e.g., N, C, S) [2,9,10], and rare earth ions doping (e.g., Nd, La, Ce) [11–14] have led to noticeably improve the photocatalytic activity of TiO_2 under visible light. Especially, doping with lanthanide ions with 4f electron configurations into TiO_2 lattice could eliminate the recombination of electron–hole pairs significantly and also result in the extension of their wavelength response toward the visible region. Recently, Li et al. [15] reported

---

* Corresponding author at: School of Resources Processing and Bioengineering, Central South University, Changsha 410083, China. Tel.: +86 731 8830543; fax: +86 731 8879815.

E-mail address: xiaoqi88@mail.csu.edu.cn (Q. Xiao).

0921-5107/$ – see front matter © 2006 Elsevier B.V. All rights reserved.
doi:10.1016/j.mseb.2006.11.011

that the band gap of TiO_2 nanoparticles was reduced by Nd^{3+} doping and the band gap narrowing was primarily attributed tot the substitution Nd^{3+} ions which introduced electron states into the band gap of TiO_2 to form the new lowest unoccupied molecular orbital. Xie and Yuan [16] reported Nd^{3+}-TiO_2 sol catalysts had photocatalytic activity for phenol degradation under visible light irradiation. Li et al. [11] reported that the introduction of Ce 4f level led to the optical absorption band between 400 and 500 nm and eliminate the recombination of electron–hole pairs and enhance the photocatalytic activity under UV or visible light illumination. But until now, there were little literatures about the effect of Sm^{3+}doping on the photocatalytic activity of TiO_2 under visible light irradiation.

Various synthetic routes like sol–gel method [12], hydrothermal method [13], coprecipitation–peptization method [14] have been studied for rare earth-doped TiO_2 nanocrystalline. Among these methods, the sol–gel process leads to the greatest possible homogeneous distribution of the dopant in the host matrix and high surface area TiO_2 particles. However, the drawback of the mentioned sol–gel route is the application of expensive raw material of tetra-isopropylorthotitanate and organic solvent, which was limited. In this work, we focus on the synthesis of Sm^{3+}-doped TiO_2 powders by sol–gel auto-combustion technique with a unique combination of the chemical sol–gel process and the combustion process. The sol–gel auto-combustion technique exploits the advantages of mixing of compositions at the level of atoms or molecules, synthesizing of ultrafine, homogeneous highly reactive powder and simple preparation method. Moreover, nanosized powders can be crystallized directly without the need for post-heat treatment, which favors high photocatalytic activity of TiO_2 nanoparticle [17,18].

In this study, high photocatalytic activity of Sm^{3+}-doped TiO_2 nanoparticles was obtained by sol–gel auto-combustion technique with the aims of: (i) extending the light absorption spectrum toward the visible region; (ii) invesgating the effect of the synthesized parameters, such as calcinations temperature and doping content of Sm^{3+} ions on the photocatalytic activity; (iii) understanding the relation between the PL spectra and the photocatalytic activity.

2. Experimental

2.1. Preparation of Sm^{3+}-doped TiO_2 nanocrystalline

Sm^{3+}-doped TiO_2 nanocrystalline was synthesized by sol–gel auto-combustion technique. The detailed process can be described as follows. The analytical grade titanium isopropoxide ($Ti(OC_2H_5)_4$), $Sm(NO_3)_3$, $C_2H_6O_2$ (ethylene glycol, EG), $C_6H_8O_7$ (citric acid, CA), ammonia (25%) and nitride acid (65–68%) were used as raw materials. Appropriate amount of $Ti(OC_2H_5)_4$ and $Sm(NO_3)_3$ were added to CA and EG mixture under constant stirring condition. The amounts of doped Sm^{3+} are 0.5–1.5 mol%. The molar ratios of CA/Ti, $NO_3{}^-$/CA and CA/EG were kept constant at 2:1, 1:1 and 1:1, respectively.

After adjusting the pH value with ammonia to 6–7, the mixture solution was evaporated at 90 °C to gradually form a clear precursor gel. The precursor gel was baked at 150 °C in muffle furnace and expanded, then was auto-ignited at about 250 °C. The puffy, porous gray powders as-combusted was calcined at the temperature of 500–800 °C for 2 h in air.

2.2. Characterization of Sm^{3+}-doped TiO_2 nanocrystalline

The crystalline structure of the samples was determined by a D/max-γA diffractometer (Cu Kα radiation, $\lambda = 0.154056$ nm) studies. The averaged grain sizes D were determined from the XRD pattern according to the Scherrer equation $D = k\lambda/\beta\cos\theta$, where k is a constant (shape factor, about 0.9), λ the X-ray wavelength (0.15418 nm), β the full width at half maximum (FWHM) of the diffraction line and θ is the diffraction angle. The values of β and θ of anatase and rutile are taken from anatase (1 0 1) and rutile (1 1 0) diffraction line, respectively. The amount of rutile in the samples were calculated using the following equation [19]: $X_R = (1 + 0.8I_A/I_R)^{-1}$, where X_R is the mass fraction of rutile in the samples, and I_A and I_R are the X-ray integrated intensities of (1 0 1) reflection of the anatase and (1 1 0) reflection of rutile, respectively.

The specific surface area of the powders was measured by the dynamic Brunauer–Emmett–Teller (BET) method, in which a N_2 gas was adsorbed at 77 K using a Micromeritics ASAP 2000 system. To study the light absorption of the photocatalyst sample, the diffuse reflectance spectra (DRS) of the photocatalyst sample in the wavelength range of 200–800 nm were obtained using a UV–vis scanning spectrophotometer (Shimadzu UV-3101), while $BaSO_4$ was as a reference. The photoluminescence (PL) spectra of the samples were recorded with a Fluorescence Spectrophotometer F-4500.

2.3. Photocatalytic activity

In order to evaluate photoactivity of the prepared samples, photocatalytic decomposition of methylene blue (MB) was performed. For a typical photocatalytic experiment, 200 mg of the prepared samples TiO_2 nanocrystalline was added to 200 mL of the 100 ppm methylene blue aqueous solution. The prepared samples TiO_2 nanocrystalline of were dispersed under ultrasonic vibration for 10 min. The suspension was kept in the dark under stirring to measure the adsorption of MB into each sample. After keeping at least 20 min, MB concentration in the solution was found to be constant on all samples prepared. Therefore, the solution in which the sample powders were dispersed was kept in the dark for 30 min and then visible light irradiation of the solution was started. For visible light irradiation, a 150 W halogen tungsten lamp with a UV and IR cut-off filter acted as a visible light source to provide light emission at 400–800 nm. After recovering the catalyst by centrifugation, the light absorption of the clear solution was measured at 660 nm (λ_{max} for MB) at a set time. The decolorization of methylene blue was calculated by formula: decolorization = $(C_0 - C)/C_0$, where C_0 and C are the concentrations of primal and photodecomposed MB. The absorbance of the MB solution was measured was measured with a UV–vis spectrophotometer (Shimadzu UV-3101).

Table 1
The characteristics of 0.5 mol% Sm^{3+}-doped TiO_2 prepared at various calcinations temperatures

Calcinations temperature (°C)	Anatase		Rutile		Specific surface area ($m^2\ g^{-1}$)	Decolourization of MB at 120 min (%)
	Crystal size, $D_{(1\,0\,1)}$ (nm)	X_A (%)	Crystal size, $D_{(1\,1\,0)}$ (nm)	X_R (%)		
500	13.1	74.7	12.8	25.3	56.00	56.39
600	13.8	48.39	13.6	51.61	52.75	67.68
700	–	5.9	14.7	94.1	49.65	65.55
800	–	0	16.3	100	45.50	50.00

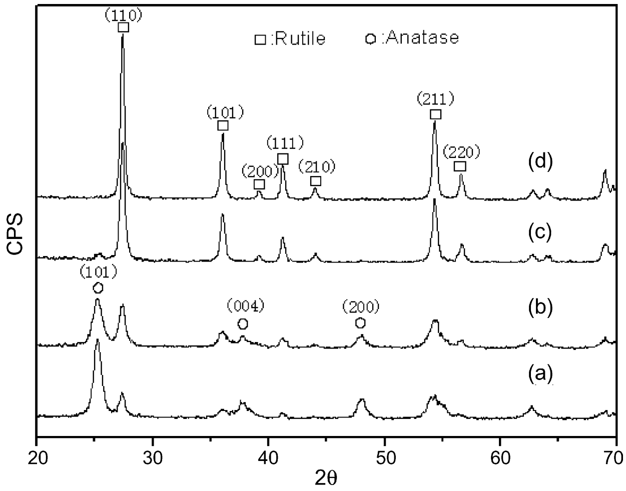

Fig. 1. XRD patterns of 0.5 mol% Sm^{3+}-doped TiO_2 with various calcined temperature: (a) 500 °C; (b) 600 °C; (c) 700 °C; (d) 800 °C.

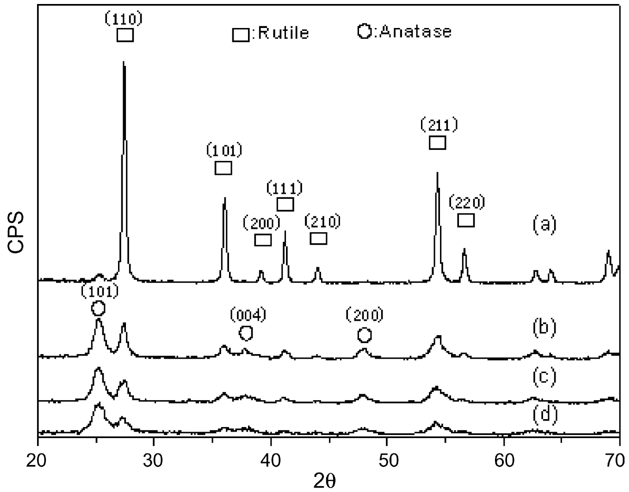

Fig. 2. XRD patterns of TiO_2 with various amounts of samarium at 600 °C for 2 h: (a) undoped; (b) 0.5 mol% Sm; (c) 1.0 mol% Sm; (d) 1.5 mol% Sm.

3. Results and discussion

3.1. XRD analysis

Fig. 1 shows the XRD patterns of TiO_2 powders doped with 0.5 mol% samarium calcined at various temperatures between 500 and 800 °C. It can be seen that no peaks from samarium oxide were observed. It was shown that the intensities of the anatase peaks decreased, while the intensities of the rutile peaks greatly increased and contents of rutile phase increased as the calcinations temperature was raised (shown in Table 1). When calcined at 800 °C, the pattern exhibits a complete rutile TiO_2 structure and it means that the phase transformation from anatase to rutile has completed at this temperature.

XRD patterns of Sm^{3+} ions-doped titania samples with various samarium content calcined at 600 °C for 2 h are shown in Fig. 2. From these XRD results, it was shown that the X-ray diffraction peak at 25.5 °C corresponds to characteristic peak of crystal plane (1 0 1) of anatase, and the peak at 27.6 °C corresponds to characteristic peak of crystal plane (1 1 0) of rutile. In undoped titania sample calcined at 600 °C for 2 h, rutile is the dominant crystallized phase, and the sample contains 97.5% of rutile phase, while Sm^{3+}-doped TiO_2 samples shows a mixture phase of anatase and rutile, and the relative ratio of rutile toanatase is reduced with the increase of samarium content, and this means that phase transition from anatase to rutile was greatly restrained by samarium ion doping (shown in Table 2).

3.2. UV–vis and PL spectra

To investigate the optical absorption properties of catalysts, we examined the diffuse reflectance spectra (DRS) of TiO_2 and

Table 2
The characteristics of Sm^{3+}-doped samples containing different samarium content calcined at 600 °C

Samarium content (%)	Anatase		Rutile		Specific surface area ($m^2\ g^{-1}$)	Decolourization of MB at 120 min (%)
	Crystal size, $D_{(1\,0\,1)}$ (nm)	X_A (%)	Crystal size, $D_{(1\,1\,0)}$ (nm)	X_R (%)		
0	–	2.41	18.8	97.59	24.52	38.71
0.5	13.8	48.39	13.6	51.61	52.75	67.68
1.0	12.9	58.22	13.1	41.78	69.48	62.02
1.5	12.5	58.33	12.8	41.67	82.94	55.94

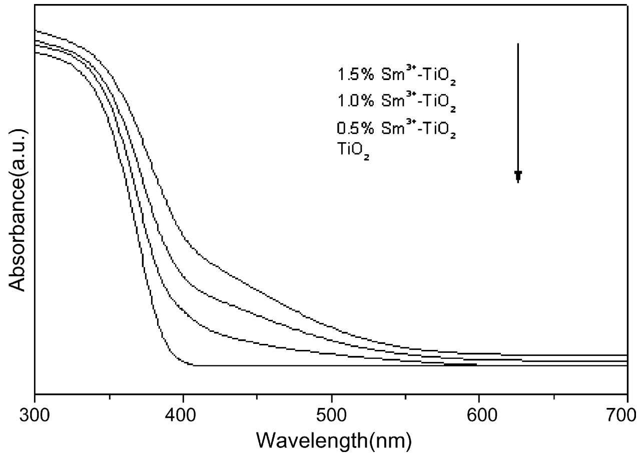

Fig. 3. UV–vis absorption spectra of pure TiO_2 and Sm^{3+}-TiO_2 calcined at 600 °C for 2 h.

Sm^{3+}-doped TiO_2 in the range of 220–850 nm and our results are shown in Fig. 3. It can be seen that while TiO_2 had no absorption in the visible region (>400 nm), Sm^{3+}-doped TiO_2 had significant absorption between 400 and 500 nm, which increased with the increase of samarium ion content. Li et al. [15] reported that the band gap of TiO_2 nanoparticles was reduced by Nd^{3+} doping and the band gap narrowing was primarily attributed to the substitution Nd^{3+} ions which introduced electron states into the band gap of TiO_2 to form the new lowest unoccupied molecular orbital. In order to understand the reason of the band gap narrowing for Sm^{3+}-doped TiO_2, density functional theory calculations were in going.

The photoluminescence emission spectra have been widely used to investigate the efficiency of charge carrier trapping, immigration and transfer and to understand the fate of electron/hole pairs in semiconductor particles [20]. In this study, Fig. 4 shows the PL spectrum of TiO_2 with various amounts of samarium at 600 °C for 2 h with the excitation wavelength of 300 nm. It can be seen that the undoped and doped TiO_2 nanoparticles can exhibit obvious excitonic PL signals with similar curve shape, demonstrating that samarium dopant does not give rise to new PL phenomena. TiO_2 nanoparticles could exhibit an obvious PL peaks at about 450 nm with the excited wavelength of 300 nm possibly resulting from binding exactions [21,22]. There were lots of oxygen vacancies on the surface of TiO_2 nanoparticles, and the size of particle was fine so that the average distance the electrons could move freely was very short. These factors could make the oxygen vacancies very easily bind electrons to form excitons. Thus, the exciton energy level near the bottom of the conduction band could come into being and the PL band of the excitons showed could also occur. Thus, the stronger the excitonic PL spectrum, the higher the content of surface oxygen vacancy and defect. In addition, the PL intensity gradually increased as samarium content increased and arrived at the highest degree when samarium content was 0.5 mol%. If samarium contents continued to increase, namely more than 0.5 mol%, the PL intensity began to go down. These results demonstrate that the content of surface oxygen vacancy arrived at the highest degree when samarium content was 0.5 mol%.

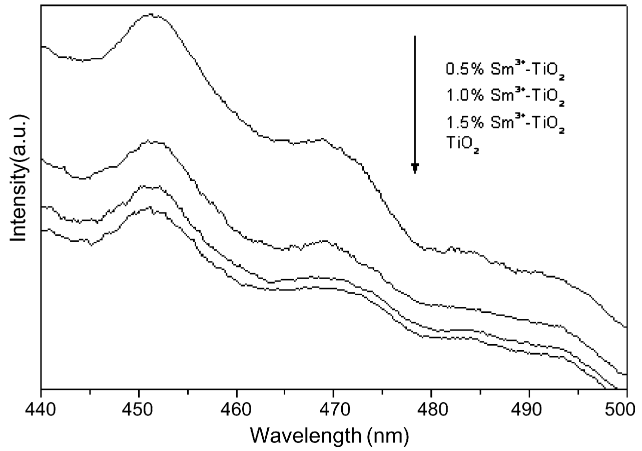

Fig. 4. PL spectrum of samarium-doped TiO_2 calcined at 600 °C for 2 h with the excitation wavelength of 300 nm.

3.3. Photocatalytic activity of Sm^{3+}-doped TiO_2 nanocrystalline

Fig. 5 shows the results of photocatalytic decomposition of methylene blue over TiO_2 doped with 0.5 mol% samarium, which were prepared at various calcinations temperatures. It is found that the photocatalytic activity is reduced considerably for the samples calcined at 800 °C and Sm^{3+}-doped TiO_2 calcined at 600 °C showed the highest photocatalytic activity among the all samples. According to the BET results (shown in Table 1), elevating the calcinations temperature reduced the specific surface areas of the catalysts. The reduction of specific surface areas means the decrease of active sites on which the reactants can adsorb. So, the increase of the calcinations temperature seems to be not helpful for the photocatalytic activity, which is not in accordance with the results of photocatalytic activity (shown in Fig. 5). Moreover, it can be seen from Table 1 that calcinations temperatures have the most significant effect on the rutile con-

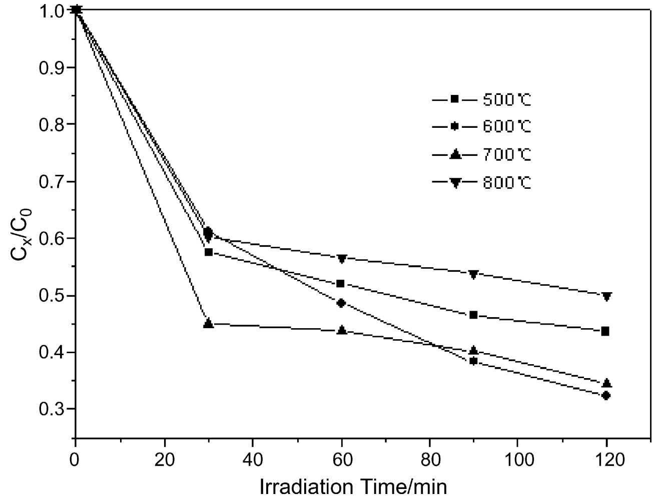

Fig. 5. Photocatalytic decomposition profiles of methylene blue. Over 0.5 mol% Sm^{3+}-doped TiO_2 nanocrystalline calcined at different temperatures.

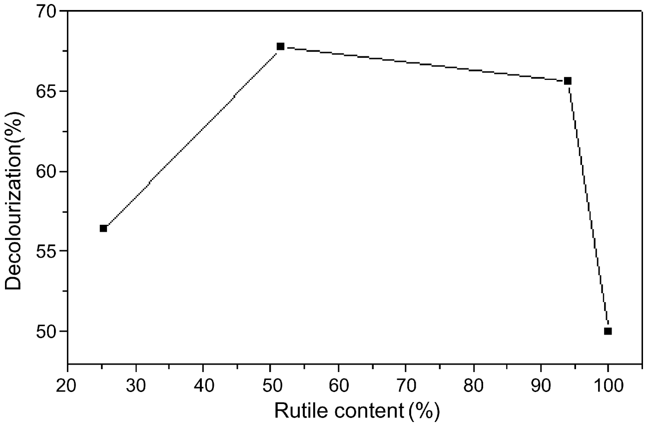

Fig. 6. Photocatalytic deodorization of methylene blue. Over 0.5 mol% Sm^{3+}-doped TiO_2 nanocrystalline containing different rutile content.

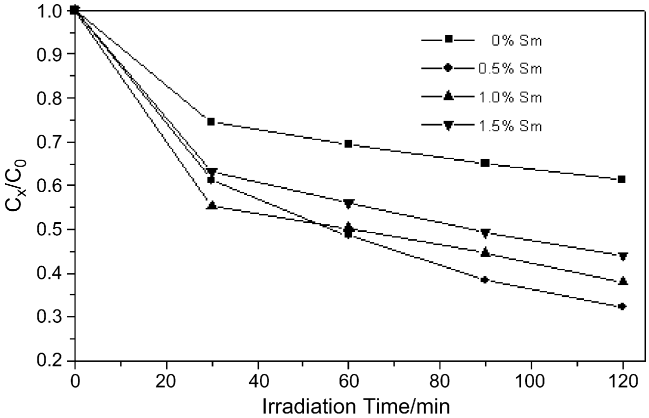

Fig. 7. Photocatalytic decomposition profiles of methylene blue. Over different samarium-doped TiO_2 nanoparticle calcined at 600 °C for 2 h.

tent, while grain size of all the samples calcinated at different temperature are nearly equal and the rutile fraction increases with increasing calcinations temperature. Recently, it has been found that a mixture of anatase and rutile TiO_2 nanoparticles has a much higher photocatalytic activity than pure anatase or pure rutile TiO_2 nanoparticles under UV light excitation [23]. The remarkable co-existent effect of rutile and anatase would arise from the increase in the charge separation efficiency due to photoinduced interfacial electron transfer from anatase to rutile under UV light excitation [24]. But until now, there were little reports about synergistic effect between anatase and rutile for doped TiO_2 samples under visible light excitation. In order to investigate the role of rutile content in photcatlytic activity for our Sm^{3+}-doped TiO_2 nanocrystalline, Fig. 6 shows the relation of the rutile content to the phtocatalytic activity of anatase and rutile TiO_2 mixture. It is clear that the photocatalytic activity of is drastically increased under the presence of a small amount of anatase phase (only 5.9% anatase) compared to pure rutile and the Sample calcinated at 600 °C consists of mixed phases with 51.61% rutile shows the highest photocatalytic activity. These results strongly suggest the existence of a synergistic effect between anatase and rutile powders in the Sm^{3+}-doped TiO_2 under visible light excitation, which is siminar to that of TiO_2 under UV light excitation [23,24].

The photocatalytic decomposition of methylene blue over Sm^{3+}-doped TiO_2 samples calcined at 600 °C was evaluated and the results are shown in Fig. 7. According to Fig. 7, the order of photocatalytic activity of samarium-doped TiO_2 nanoparticles at 120 min was as following: $0.5 > 1.0 > 1.5 > 0$ mol%, which suggests that the Sm^{3+} doping enhances the photocatalytic activity of TiO_2 and there is an optimum doping content of Sm^{3+} ions in TiO_2 particles.

Some studies indicated that the photocatalytic activity of TiO_2 catalysts depends strongly on two factors: adsorption behavior and the separation efficiency of electron–hole pairs [3,25,26].

On the one hand, the BET results showed that the specific surface areas of the catalysts increased from 24.52 $m^2\,g^{-1}$ for TiO_2 to 82.94 $m^2\,g^{-1}$ for 1.5% Sm^{3+}-TiO_2 significantly (shown in Table 2). The larger specific surface area of Sm^{3+}-TiO_2 catalysts would be beneficial to achieve better adsorption of MB in aqueous suspension. Therefore, the increase of samarium ion content seems to be helpful for the photocatalytic activity. According to Fig. 7 and Table 2, the photocatalytic reactivity of Sm^{3+}-TiO_2 is higher than that of undoped TiO_2, which is consistent with the larger specific surface area of Sm^{3+}-TiO_2 than undoped TiO_2. However, it was noticeable that a larger specific surface area of Sm^{3+}-TiO_2 with a higher samarium ion dosage did not lead to a higher photocatalytic activity, which might be limited by lower separation efficiency of electron–hole pairs.

On the other hand, according to Figs. 4 and 7, it should be pointed that the order of photocatalytic activity was the same as that of PL intensity, namely, the stronger the PL intensity, the higher the photocatalytic activity. From Table 2, it can be seen that samarium doping content has little influence on grain size and rutile content of all the samples. Xu et al. [27] reported that there exists an optimum doping content of rare earth ions in TiO_2 particles for the most efficient separation of photoinduced electron–hole pairs. During the process of PL, oxygen vacancies and defects could bind photoinduced electrons to form free or binding exactions so that PL signal could easily occur, and the larger the content of oxygen vacancies or defects, the stronger the PL intensity. But, during the process of photocatalytic reactions, oxygen vacancies and defects could become the centers to capture photoinduced electrons so that the recombination of photoinduced electrons and holes could be effectively inhibited. Moreover, oxygen vacancies could promote the adsorption of O_2, and there was strong interaction between the photoinduced electrons bound by oxygen vacancies and adsorbed O_2. This indicated that the binding for photoinduced electrons of oxygen vacancies could make for the capture for photoinduced electrons of adsorbed O_2, and O_2 free group was produced at the same time. Thus, oxygen vacancies and defects were in favor of photocatalytic reactions in that O_2 was active to promote the oxidation of organic substances [3,28]. The above results demonstrated that there were certain relationships between PL spectra and photocatalytic activity, namely, the stronger the PL intensity, the larger the content of oxygen vacancies and defects, the higher the photocatalytic activity. Therefore, in this study, 0.5 mol% may be the most suitable content of Sm^{3+} in the titania, at which the recombination of photoinduced electrons and holes could be effectively inhibited and thereby the highest photocatalytic activity is formed.

4. Conclusion

High photocatalytic activity of Sm^{3+}-doped TiO_2 nanocrystalline under visible light has been successfully prepared by sol–gel auto-combustion technique. UV–vis diffuse reflectance spectra showed a slight shift to longer wavelengths and an extension of the absorption in the visible region for almost all the samarium-doped samples, compared to the non-doped sample. The results of photocatalytic decomposition of methylene blue over 0.5 mol% Sm^{3+}-TiO_2 prepared at various calcinations temperatures show that the Sample calcinated at 600 °C consists of mixed phases with 51.61% rutile shows the highest photocatalytic activity, which suggests the existence of a synergistic effect between anatase and rutile powders under visible light. Doping with the samarium ions significantly enhanced the overall photocatalytic activity for MB degradation under visible light irradiation because the larger specific surface area and the higher separation efficiency of electron–hole pairs were obtained simultaneously for Sm^{3+}-doped TiO_2 nanocrystalline. There were certain relationships between PL spectra and photocatalytic activity, namely, the stronger the PL intensity, the larger the content of oxygen vacancies and defects, the higher the photocatalytic activity. Therefore, in this study, 0.5 mol% may be the most suitable content of Sm^{3+} in the titania, at which the recombination of photoinduced electrons and holes could be effectively inhibited and thereby the highest photocatalytic activity is formed.

Acknowledgements

This work was supported by the Provincial Excellent Ph.D. Thesis Research Program of Hunan (No. 2004-141) and the Postgraduate Educational Innovation Engineering of Central South University (No. 2005-22). The authors are grateful to Dr. Huang Suping for her encouragement and helpful discussion.

References

[1] A. Fujishima, K. Honda, Nature 238 (1972) 37.
[2] R. Asahi, T. Morikawa, T. Ohwaki, K. Aoki, Y. Taga, Science 293 (2001) 269.
[3] M.R. Hoffmann, S.T. Martin, W. Choi, D.W. Bahnemann, Chem. Rev. 95 (1995) 69.
[4] B. Mahrov, G. Boschloo, A. Hagfeldt, Appl. Phys. Lett. 84 (2004) 5455.
[5] A. Hattori, Y. Tokihisa, H. Tada, S. Ito, J. Electrochem. Soc. 147 (2000) 2279.
[6] C. Wang, B. Xu, X. Wang, J. Zhao, J. Solid State Chem. 178 (2005) 3500.
[7] H. Yamashita, M. Harada, J. Misaka, M. Takeuchi, B. Neppolian, M. Anpo, Catal. Today 84 (2003) 191.
[8] D.H. Kim, S.I. Woo, S.H. Moom, H.D. Kim, B.Y. Kim, J.H. Cho, Y.G. Joh, E.C. Kim, Solid State Commun. 136 (2005) 554.
[9] H. Kamisaka, T. Adachi, K. Yamashita, J. Chem. Phys. 123 (2005) 084704.
[10] K. Madhusudan Reddy, B. Baruwati, M. Jayalakshmi, M. Mohan Rao, S.V. Manorama, J. Solid Chem. 178 (2005) 3352.
[11] F.B. Li, X.Z. Li, M.F. Hou, K.W. Cheah, W.C.H. Choy, Appl. Catal. A: Gen. 285 (2005) 181.
[12] Y. Zhang, H. Xu, Y. Xu, H. Zhang, Y. Wang, J. Photochem. Photobiol. A: Chem. 170 (2005) 279.
[13] X. Yan, J. He, D. Evans, X. Duan, Y. Zhu, Appl. Catal. B: Environ. 55 (2005) 243.
[14] Y. Xie, C. Yuan, X. Li, Mater. Sci. Eng. B 117 (2005) 325.
[15] W. Li, Y. Wang, H. Lin, S. Ismat Shah, C.P. Doren, S.A. Rykov, J.G. Chen, M.A. Barteau, Appl. Phys. Lett. 83 (2003) 4143.
[16] Y. Xie, C. Yuan, Appl. Surf. Sci. 221 (2004) 17.
[17] G. Sivalingam, G. Madras, Appl. Catal. A: Gen. 269 (2004) 81.
[18] K. Nagaveni, G. Sivalingam, M.S. Hegde, G. Madras, Appl. Catal. B: Environ. 48 (2004) 83.
[19] R.A. Spurr, H. Myers, Anal. Chem. 29 (1957) 760.
[20] H. Yamashita, Y. Ichihashi, S.G. Zhang, Y. Matrumura, Y. Souma, T. Tatsumi, M. Anpo, Appl. Surf. Sci. 121/122 (1997) 305.
[21] L. Zhang, C. Mo, Nanostruct. Mater. 6 (1995) 831.
[22] D. Li, Y. Zhen, X. Fu, Chin. J. Mater. Res. 14 (2000) 639.
[23] D.C. Hurum, A.G. Agrios, K.A. Gray, T. Rajh, M.C. Thurnauer, J. Phys. Chem. B 107 (2003) 4545.
[24] T. Miyagi, M. Kamei, T. Mitsuhashi, T. Ishigaki, A. Yamazaki, Chem. Phys. Lett. 390 (2004) 399.
[25] A. Fujishima, T.N. Rao, D.A. Tryk, J. Photochem. Photobiol. C: Photochem. Rev. 1 (2000) 1.
[26] P.V. Kamat, Chem. Rev. 93 (1993) 267.
[27] A.-W. Xu, Y. Gao, H.-Q. Liu, J. Catal. 207 (2002) 151.
[28] H. Liu, S. Cheng, M. Wu, H. Wu, J. Zhang, W. Li, C. Cao, J. Phys. Chem. A 104 (2000) 7016.